

# Pion and $\rho$ -meson screening masses at finite chemical potential in two-flavor lattice QCD with Wilson fermion

Junpei Sugano,<sup>1,\*</sup> Junichi Takahashi,<sup>2</sup> Hiroaki Kouno,<sup>3</sup> and Masanobu Yahiro<sup>1</sup>

<sup>1</sup>*Department of Physics, Graduate School of Sciences, Kyushu University, Fukuoka 819-0395, Japan*

<sup>2</sup>*Division of Observation, Fukuoka Aviation Weather Station,  
Japan Meteorological Agency, Fukuoka 812-0005, Japan*

<sup>3</sup>*Department of Physics, Saga University, Saga 840-8502, Japan*

(Dated: September 11, 2017)

We investigate the real and the imaginary chemical-potential ( $\mu$ ) dependence of pion and  $\rho$ -meson screening masses in both the confinement and the deconfinement region by using two-flavor lattice QCD. The spatial meson correlators are calculated in the imaginary  $\mu$  region with lattice QCD simulations on an  $8^2 \times 16 \times 4$  lattice with the clover-improved two-flavor Wilson fermion action and the renormalization-group-improved Iwasaki gauge action. We extract pion and  $\rho$ -meson screening masses from the correlators. The meson screening masses thus obtained are extrapolated to the real  $\mu$  region by assuming either the Fourier or the polynomial series. In the real  $\mu$  region, the resulting pion and  $\rho$ -meson screening masses monotonically increase as real  $\mu$  becomes large.

## I. INTRODUCTION

Understanding of the QCD phase diagram [1–3] is a long-standing issue in hadron physics. The knowledge of thermal properties of the QCD is essential to clarify the phase diagram, and lattice QCD (LQCD) simulations are well established as a powerful tool. Indeed, LQCD simulations are successful in clarifying the phase diagram and the properties of QCD at zero chemical potential ( $\mu$ ) and finite temperature ( $T$ ) [4]. It is, however, difficult to perform LQCD simulations for finite real  $\mu$ , since the fermion determinant  $\det\mathcal{M}(\mu)$  becomes complex:

$$(\det\mathcal{M}(\mu))^* = \det\mathcal{M}(-\mu^*) = \det\mathcal{M}(-\mu). \quad (1)$$

This is the well-known sign problem. It prevents us from using Monte-Carlo methods based on the importance sampling.

Several methods were proposed so far, in order to circumvent the sign problem [5], e.g., the Taylor expansion method [6–8], the reweighting method [9], the analytic continuation from the purely-imaginary  $\mu$  region to the real  $\mu$  region [10, 11], and the canonical approach [12–14]. Recently, the complex Langevin method [15–18] and the Lefschetz thimble theory [19, 20] were proposed as the new methods, and made a great progress. Among these methods, we focus on the imaginary  $\mu$  approach in this paper. For purely-imaginary chemical potential  $\mu = i\mu_I = i\theta T$ , the first equality of Eq. (1) ensures that the fermion determinant  $\det\mathcal{M}(i\theta T)$  is real. Here,  $\theta$  is a dimensionless chemical potential. This means that LQCD simulations can be performed with usual Monte-Carlo methods for finite  $\theta$ . Observables calculated at  $\theta = \mu_I/T$  are analytically continued to real  $\mu/T$  ( $\mu_R/T$ ), by assuming that the  $\theta$  dependence of observables can be described by some analytic function.

Toward the clarification of the QCD phase diagram, meson screening masses are extensively calculated by using LQCD

simulations [21–23]. Indeed, the meson screening masses are good indicators to see chiral and  $U_A(1)$  symmetry restorations [24, 25], and hence essential quantities to explore the QCD phase diagram. It is also expected that the meson screening masses play a key role in investigating medium properties of hadronic excitations in the Quark Gluon Plasma [26] that may be created by relativistic heavy-ion collision experiments. As for finite  $\mu_R$ , pion and  $\rho$ -meson screening masses were calculated up to order  $(\mu_R/T)^2$  with the Taylor expansion method for both staggered-type fermions [27] and Wilson-type ones [28].

In this paper, we investigate the  $\mu$  dependence of pion and  $\rho$ -meson screening masses in both the imaginary and the real  $\mu$  region by using two-flavor LQCD simulations. We first calculate the spatial pion and  $\rho$ -meson correlators in the purely-imaginary  $\mu$  region, i.e., the  $\theta$  region. The simulations can be made with standard numerical prescriptions, since there is no sign problem in the  $\theta$  region. The calculated correlators are fitted by the exponential form at large distance, in order to derive the screening masses. To perform the analytic continuation from the imaginary to the real  $\mu$  region, we fit the resulting meson screening masses by the Fourier or the polynomial series in the  $\theta$  region. After the fitting, the meson screening masses at finite  $\mu_R/T$  are extracted by taking the replacement  $\theta \rightarrow -i\mu_R/T$  in the series.

Actual LQCD simulations are done on an  $8^2 \times 16 \times 4$  lattice with the clover-improved two-flavor Wilson fermion action and the renormalization-group-improved Iwasaki gauge action. We adopt the line of constant physics with  $m_{PS}/m_V = 0.80$  obtained in Refs. [29–31] for finite-temperature simulations, where  $m_{PS}$  and  $m_V$  are pseudoscalar-meson and vector-meson masses, respectively. Three temperatures  $T/T_{pc} = 0.93, 1.08, \text{ and } 1.35$  are considered. The pseudocritical temperature at  $\mu = 0$  is represented by  $T_{pc}$  [8, 30]. We compute spatial pion and  $\rho$ -meson correlators at these temperatures and in the range  $0 \leq \theta \leq \pi/3$ . We generated about 32,000 trajectories and removed the first 4,000 trajectories for the thermalization of  $T$  and  $\theta$ , and then measured pion and  $\rho$ -meson correlators at every 100 trajectories. Lattice gauge

\*sugano@phys.kyushu-u.ac.jp

configurations taken above are the same as in our previous work [32] where the quark number density was analyzed.

The rest of this paper is organized as follows. In Sec. II, we explain the meson screening mass and the analytic continuation. In Sec. III, we show numerical results for the meson screening masses at both imaginary and real  $\mu$ . Section IV is devoted to a summary.

## II. FORMULATION

In this section, we explain the formulation of meson screening mass and analytic continuation from the  $\theta$  region to the  $\mu_R/T$  region. As for LQCD setup, see Ref. [32].

### A. Meson screening mass

We extract pion and  $\rho$ -meson screening masses at finite  $\theta$  from the spatial correlator

$$C_i(z; T, \theta) = \sum_{x, y, t} \langle M_i(x, y, z, t) M_i^\dagger(0, 0, 0, 0) \rangle, \quad (2)$$

with the meson operator

$$M_i(x, y, z, t) \equiv \bar{q}(x, y, z, t) \Gamma_i \tau^a q(x, y, z, t), \quad (3)$$

where the subscript  $i$  represents the species of meson,  $\tau^a$  is the Pauli matrix in flavor space, and  $\Gamma_\pi = \gamma_5$  for pion and  $\Gamma_\rho = \gamma_\mu$  for  $\rho$ -meson. The correlator is summed over  $x, y, t$  in order to project on zero momenta in the  $x$ - and  $y$ -directions and on zero energy in the  $t$ -direction.

Considering large  $z$ , we derive the meson screening mass  $m_i(T, \theta)$  from  $C_i(z; T, \theta)$  by fitting it with the exponential form:

$$C_i(z; T, \theta) = A_i(T, \theta) \left( e^{-m_i(T, \theta)z} + e^{-m_i(T, \theta)(N_z - z)} \right), \quad (4)$$

where  $A_i(T, \theta)$  is the fitting parameter together with  $m_i(T, \theta)$ , and  $N_z$  is the lattice size in the  $z$ -direction. The correlator (2) is charge-even. This ensures that  $m_i(T, \theta)$  is also charge-even and real, even when the chemical potential is purely imaginary. In fact, we have confirmed that the calculated correlator has no imaginary part.

### B. Analytic continuation

Our goal is to obtain the meson screening mass at  $\mu_R/T$ . We then extrapolate the calculated  $m_i(T, \theta)$  to the  $\mu_R/T$  region, assuming some analytic function for each temperature taken. In this paper, we consider three temperatures, e.g.,  $T/T_{pc} = 0.93, 1.08$  and  $1.35$ . Figure 1 shows the phase diagram in  $T$ - $\theta$  plane. The arrows present three cases of  $T/T_{pc} = 0.93, 1.08$  and  $1.35$ . The system is in the confinement region at  $T/T_{pc} = 0.93$ , and in the deconfinement region at  $T/T_{pc} = 1.35$  for any  $\theta$  in  $0 \leq \theta \leq \pi/3$ . As for

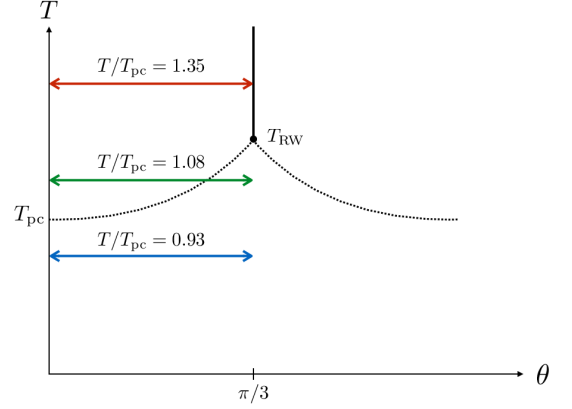


Fig. 1: Sketch of the phase diagram in the  $\theta$  region. The dotted line denotes the pseudocritical line, and the solid line does the first-order Roberge-Weiss transition line. The symbols  $T_{pc}$  and  $T_{RW}$  mean the pseudocritical temperature at  $\theta = 0$  and the endpoint temperature of the Roberge-Weiss transition at  $\theta = \pi/3$ , respectively. The arrows indicate three cases of  $T/T_{pc} = 0.93, 1.08$  and  $1.35$ .

$T/T_{pc} = 1.08$ , it was found in our previous work [32] that the temperature satisfies  $T_{pc} < T < T_{RW}$ , where  $T_{RW}$  corresponds to the endpoint of the first-order Roberge-Weiss (RW) transition [33]. This means that the system changes from the deconfinement region to the confinement one at some value  $\theta = \theta_c$ .

In determining the reasonable analytic function for each temperature, the behavior of physical quantity  $\mathcal{O}(T, \theta)$  in the  $\theta$  region is essential. For  $T < T_{pc}$ , it is found that  $\mathcal{O}(T, \theta)$  is a smooth function of  $\theta$  and has a periodicity of  $2\pi/3$  in  $\theta$  [33–37]. From this point of view, we use the Fourier series for  $T/T_{pc} = 0.93$  as an extrapolation function,

$$\frac{m_i(T, \theta)}{T} = G_{F,i}^n(T, \theta) = \sum_{k=0}^n a_{F,i}^{(k)}(T) \cos(3k\theta), \quad (5)$$

where  $n$  denotes the highest order of series. The function  $\sin(3k\theta)$  does not appear in Eq. (5) because both  $m_\pi$  and  $m_\rho$  are charge-even. Then, the screening mass in the  $\mu_R/T$  region is obtained by the analytic continuation, that is, by the replacement  $\theta \rightarrow -i\mu_R/T$ :

$$\begin{aligned} \frac{m_i(T, \mu_R/T)}{T} &= H_{F,i}^n \left( T, \frac{\mu_R}{T} \right) \\ &= \sum_{k=0}^n a_{F,i}^{(k)}(T) \cosh \left( 3k \frac{\mu_R}{T} \right). \end{aligned} \quad (6)$$

Note that the coefficients  $a_{F,i}^{(k)}(T)$  in Eq. (6) have already been determined in the  $\theta$  region. This is true for other temperatures.

As for  $T_{pc} < T$ , two cases can be considered; one is  $T_{RW} < T$  and the other is  $T_{pc} < T < T_{RW}$ . For  $T_{RW} < T$ , the first-order RW phase transition takes place at  $\theta = \pi/3$  [33], and analyticity of  $\mathcal{O}(T, \theta)$  is lost. Indeed, on the RW phase transition line, a cusp comes out for charge-even

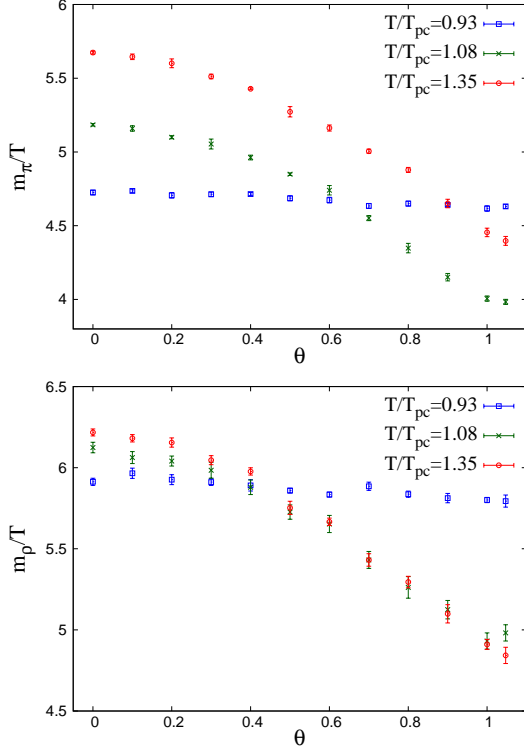


Fig. 2: The  $\theta$  dependence of pion and  $\rho$ -meson screening masses for all the  $T$  we consider. The LQCD data are shown by symbols with error bars.

$\mathcal{O}(T, \theta)$  [34–37] such as  $m_i(T, \theta)$ . This indicates that  $\mathcal{O}(T, \theta)$  monotonically increases or decreases in the region  $[0, \pi/3]$ . As for  $T/T_{pc} = 1.35$ , therefore, the polynomial series including only even powers is applied to extrapolate  $m_i(T, \theta)/T$  to the  $\mu_R/T$  region:

$$\frac{m_i(T, \theta)}{T} = G_{P,i}^n(T, \theta) = \sum_{k=0}^n a_{P,i}^{(k)}(T) \theta^{2k}. \quad (7)$$

After the replacement  $\theta \rightarrow -i\mu_R/T$ , we can obtain

$$\begin{aligned} \frac{m_i(T, \mu_R/T)}{T} &= H_{P,i}^n \left( T, \frac{\mu_R}{T} \right) \\ &= \sum_{k=0}^n (-1)^k a_{P,i}^{(k)}(T) \left( \frac{\mu_R}{T} \right)^{2k}. \end{aligned} \quad (8)$$

For  $T/T_{pc} = 1.08$ , the system is in the deconfinement region  $\theta \leq \theta_c$ , while the confinement is realized for  $\theta > \theta_c$ . It is thus unclear which analytic function is suitable. Hence, for  $T/T_{pc} = 1.08$ , we consider the region  $0 \leq \theta \leq \theta_c$  only, and take the polynomial series (7). The actual value of  $\theta_c$  is determined later.

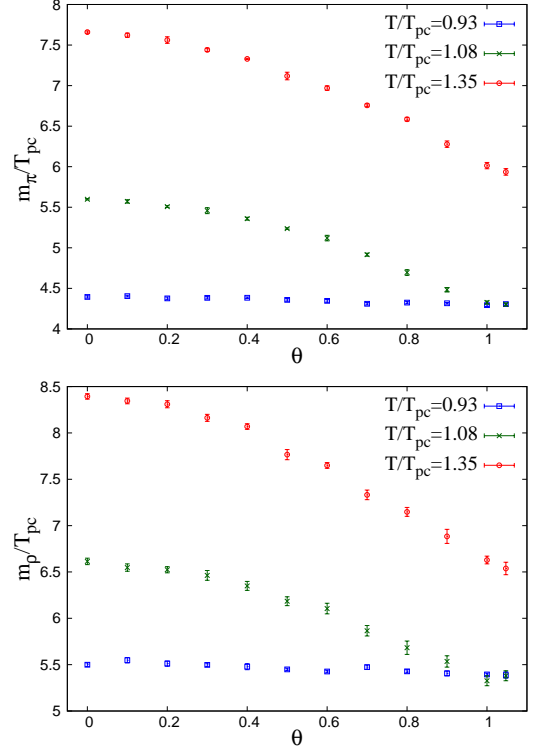


Fig. 3: The  $\theta$  dependence of pion and  $\rho$ -meson screening masses divided by  $T_{pc}$ . The meaning of symbols is the same as in Fig. 2.

### III. NUMERICAL RESULTS

#### A. Meson screening mass at imaginary $\mu$

Figure 2 shows pion and  $\rho$ -meson screening masses as a function of  $\theta$  for all the  $T$  we consider; our LQCD data are plotted by symbols with error bars. The  $\theta$  dependence of the screening masses at  $T/T_{pc} = 0.93$  is quite small. This suggests that the system is in the chiral symmetry broken phase at  $T/T_{pc} = 0.93$ . On the contrary, for  $T/T_{pc} = 1.08$  and  $T/T_{pc} = 1.35$ , the  $\theta$  dependence of the screening masses are remarkable, and this behavior indicates realization of the chiral symmetry restoration.

In Fig. 3, pion and  $\rho$ -meson screening masses divided by  $T_{pc}$  are plotted as a function of  $\theta$ . In both the panels, the value of screening mass at  $T/T_{pc} = 1.08$  almost agree with that at  $T/T_{pc} = 0.93$ , when  $\theta = \theta_c > 0.8$ . This means that the system is in the deconfinement region for  $\theta \leq \theta_c$ , whereas the confinement takes place for  $\theta > \theta_c$ . Therefore, for  $T/T_{pc} = 1.08$ , we use the data only in the range  $0 \leq \theta \leq 0.8$  for the extrapolation to the  $\mu_R/T$  region, and the polynomial series (7) as an extrapolation function.

#### B. Fitting of meson screening mass at imaginary $\mu$

Now, we perform the  $\chi^2$  fitting for LQCD data on screening masses in the  $\theta$  region. We first consider the case of

TABLE I: Coefficients of the Fourier series at  $T/T_{\text{pc}} = 0.93$ .

| meson         | $T/T_{\text{pc}}$ | $a_{\text{F},i}^{(0)}$ | $a_{\text{F},i}^{(1)}$ | $a_{\text{F},i}^{(2)}$ | $\chi^2/\text{dof}$ |
|---------------|-------------------|------------------------|------------------------|------------------------|---------------------|
| pion          | 0.93              | 4.682(4)               | 0.05210(557)           | —                      | 0.582               |
|               | 0.93              | 4.683(4)               | 0.05170(562)           | -0.002999(5851)        | 0.617               |
| $\rho$ -meson | 0.93              | 5.867(6)               | 0.06103(915)           | —                      | 0.897               |
|               | 0.93              | 5.867(6)               | 0.06163(925)           | 0.003645(7942)         | 0.974               |

TABLE II: Coefficients of the polynomial series at  $T/T_{\text{pc}} = 1.08$ . Note that the fitting is performed only in the range  $0 \leq \theta \leq 0.8$ .

| meson         | $T/T_{\text{pc}}$ | $a_{\text{P},i}^{(0)}$ | $a_{\text{P},i}^{(1)}$ | $a_{\text{P},i}^{(2)}$ | $\chi^2/\text{dof}$ |
|---------------|-------------------|------------------------|------------------------|------------------------|---------------------|
| pion          | 1.08              | 5.171(6)               | -1.279(26)             | —                      | 1.099               |
|               | 1.08              | 5.173(6)               | -1.326(73)             | 0.1014(1474)           | 1.203               |
| $\rho$ -meson | 1.08              | 6.098(19)              | -1.335(77)             | —                      | 0.340               |
|               | 1.08              | 6.103(21)              | -1.450(247)            | 0.2153(4416)           | 0.357               |

$T/T_{\text{pc}} = 0.93$ , and fit pion and  $\rho$ -meson screening masses by the Fourier series (5). We perform the  $\chi^2$  fitting by using  $G_{\text{F},i}^1$  and  $G_{\text{F},i}^2$  because the resulting screening masses have small  $\theta$  dependence, as shown in Fig. 2.

The coefficients obtained from the  $\chi^2$  fitting are tabulated in Table I, together with the value of  $\chi^2$  degree of freedom (dof). For both pion and  $\rho$ -meson, the values of  $a_{\text{F},i}^{(2)}$  have large error bars, indicating that the  $a_{\text{F},i}^{(2)}$  cannot be determined precisely from the present LQCD data. Hence, we use  $G_{\text{F},i}^1$  only for the extrapolation at  $T/T_{\text{pc}} = 0.93$ . In Fig. 4, we plot the fitting result in which two lines correspond to the upper and lower bounds of fitting.

Next, we consider the cases of  $T/T_{\text{pc}} = 1.08$  and 1.35. The polynomial series  $G_{\text{P},i}^n$  is used for the fitting. Indeed, the  $m_i(T, \theta)/T$  in Fig. 2 are monotonically decreasing. This suggests that the polynomial fitting works well. As the fitting functions, we take  $G_{\text{P},i}^1$  and  $G_{\text{P},i}^2$  for  $T/T_{\text{pc}} = 1.08$  and  $G_{\text{P},i}^1$ ,  $G_{\text{P},i}^2$  and  $G_{\text{P},i}^3$  for  $T/T_{\text{pc}} = 1.35$ .

For the case of  $T/T_{\text{pc}} = 1.08$ , the coefficients and the  $\chi^2/\text{dof}$  after the fitting are summarized in Table II. In this case, the data are taken only in the range  $0 \leq \theta \leq 0.8$ , as already mentioned above. The errors of  $a_{\text{P},i}^{(2)}$  have the same order as the corresponding mean values, although the  $\chi^2/\text{dof}$  is slightly improved for  $\rho$ -meson. The coefficient  $a_{\text{P},i}^{(2)}$  cannot be determined clearly from the present LQCD data, and hence we take  $G_{\text{P},i}^1$  only as a good fitting function for  $T/T_{\text{pc}} = 1.08$ , and extrapolate the  $G_{\text{P},i}^1$  to the  $\mu_{\text{R}}/T$  region. Figure 5 shows the fitting result in which the upper and lower bounds of fitting are also plotted.

Table III presents the obtained coefficients and the  $\chi^2/\text{dof}$  for  $T/T_{\text{pc}} = 1.35$ . From Table III, the errors of  $a_{\text{P},i}^{(3)}$  are large and same order of the corresponding mean values. In addition, the value of  $\chi^2/\text{dof}$  is considerably improved when the  $G_{\text{P},i}^2$  is used for the fitting function, instead of the  $G_{\text{P},i}^1$ . Hence, we use the  $G_{\text{P},i}^2$  as an extrapolation function for  $T/T_{\text{pc}} = 1.35$ . The fitting result is presented in Fig. 6.

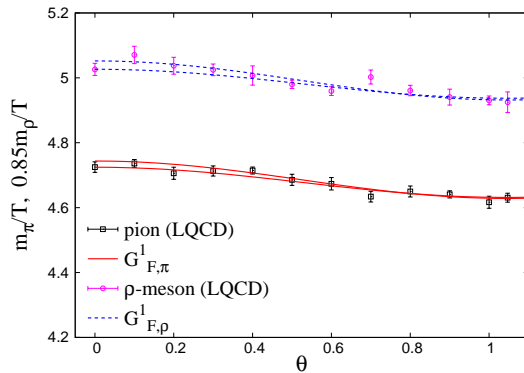


Fig. 4: Fitting results of pion and  $\rho$ -meson screening masses at  $T/T_{\text{pc}} = 0.93$ . The Fourier series is used for the fitting. Here,  $m_\rho/T$  is multiplied by 0.85.

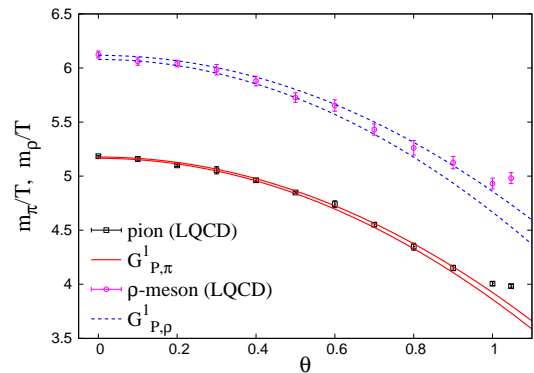
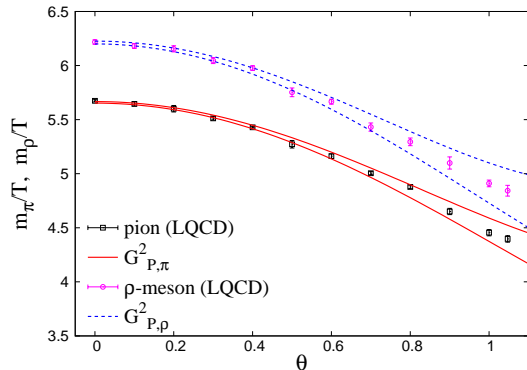


Fig. 5: The polynomial fitting results of pion and  $\rho$ -meson screening masses at  $T/T_{\text{pc}} = 1.08$ . Note that the fitting is performed by using the data only in  $0 \leq \theta \leq 0.8$ .

TABLE III: Coefficients of the polynomial series at  $T/T_{pc} = 1.35$ .

| meson         | $T/T_{pc}$ | $a_{p,i}^{(0)}$ | $a_{p,i}^{(1)}$ | $a_{p,i}^{(2)}$ | $a_{p,i}^{(3)}$ | $\chi^2/\text{dof}$ |
|---------------|------------|-----------------|-----------------|-----------------|-----------------|---------------------|
| pion          | 1.35       | 5.633(6)        | -1.208(16)      | —               | —               | 4.332               |
|               | 1.35       | 5.660(7)        | -1.473(49)      | 0.2950(520)     | —               | 1.203               |
|               | 1.35       | 5.669(9)        | -1.641(99)      | 0.7804(2530)    | -0.3286(1677)   | 0.905               |
| $\rho$ -meson | 1.35       | 6.179(11)       | -1.316(26)      | —               | —               | 2.932               |
|               | 1.35       | 6.213(13)       | -1.711(86)      | 0.4119(868)     | —               | 0.695               |
|               | 1.35       | 6.210(14)       | -1.644(191)     | 0.2084(5233)    | 0.1382(3506)    | 0.762               |

Fig. 6: The polynomial fitting results of pion and  $\rho$ -meson screening masses at  $T/T_{pc} = 1.35$ .

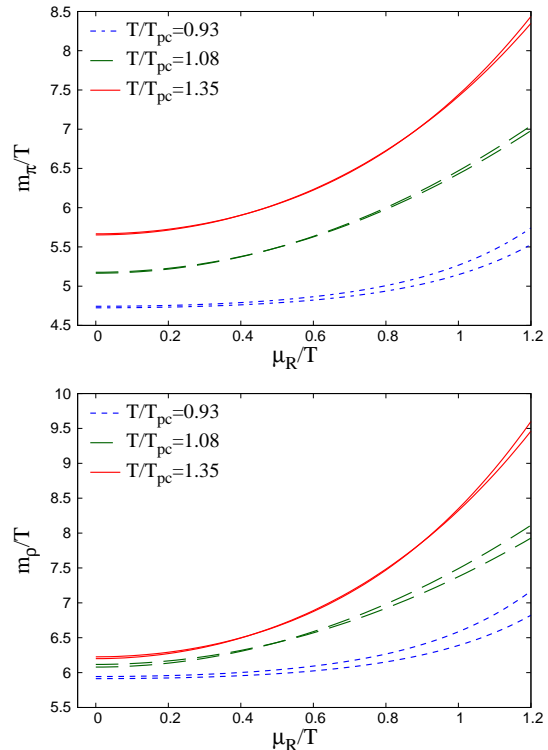
### C. Meson screening masses at $\mu_R/T$

After the replacement  $\theta \rightarrow -i\mu_R/T$ , we can obtain the meson screening masses at finite  $\mu_R/T$ ; as for the extrapolated functional form, see Eqs. (6) and (8). Figure 7 shows the resulting  $\mu_R/T$  dependence of pion and  $\rho$ -meson screening masses for three temperatures. At  $\mu_R/T = 0$ , pion screening mass is sensitive to temperature, while  $\rho$ -meson screening mass is not. This result is reasonable since  $\rho$ -meson is heavier than pion. In addition, as  $\mu_R/T$  increases, pion and  $\rho$ -meson screening masses are monotonically increasing in all the temperatures.

In our previous work [32] on the quark number density, the result of the imaginary- $\mu$  approach is consistent with the one obtained from the Taylor expansion method up to  $\mu_R/T \sim 0.8$  at low temperature. In this range, the screening masses are almost constant for  $T/T_{pc} = 0.93$ , and this indicates that the chiral symmetry is not restored. Meanwhile, the  $\mu_R/T$  dependence is remarkable for  $T/T_{pc} = 1.08$  and 1.35 because of the chiral symmetry restoration.

## IV. SUMMARY

In this paper, we investigated the  $\mu$  dependence of pion and  $\rho$ -meson screening masses in the imaginary and real regions by using LQCD simulations. Meson correlators were calculated at imaginary  $\mu$  by using LQCD simulations on an

Fig. 7: The  $\mu_R/T$  dependence of the pion and  $\rho$ -meson screening masses. The functional form is represented in Eqs. (6) and (8).

$8^2 \times 16 \times 4$  lattice with the clover-improved two-flavor Wilson fermion action and the renormalization-group-improved Iwasaki gauge action. Next, the meson correlators were fitted by the exponential form at large  $z$ , and thereby the meson screening masses were extracted as a function of  $\theta$  for  $T/T_{pc} = 0.93, 1.08$  and 1.35; note that the system is in the confinement (deconfinement) phase for  $T/T_{pc} = 0.93$  (1.35) and at  $T/T_{pc} = 1.08$  it is in the confinement phase for small  $\theta$  and the deconfinement phase for large  $\theta$ .

To obtain the  $\mu_R/T$  dependence of the screening masses by the analytic continuation, we fitted the LQCD data by the analytic function; the Fourier series was used for the case of  $T/T_{pc} = 0.93$ , while the polynomial series was applied for  $T/T_{pc} = 1.08, 1.35$ . From the fitting, we found that the higher-order contributions become important as  $T$  increases. Finally, the meson screening masses are extrapolated to the

$\mu_R/T$  region by the replacement  $\theta \rightarrow -i\mu_R/T$ . It is found that, for all the  $T$  we took, the pion and  $\rho$ -meson screening masses are monotonically increasing as  $\mu_R/T$  becomes large.

### Acknowledgments

We thank A. Nakamura and K. Nagata for useful discussions and giving the LQCD program codes. J.S., H. K., and M.

Y. are supported by Grant-in-Aid for Scientific Research (No. 27-7804, No. 26400279, No. 17K05446, and No. 26400278) from the Japan Society for the Promotion of Science (JSPS). The numerical calculations were performed on NEC SX-ACE at CMC, Osaka University.

- 
- [1] P. Braun-Munzinger and J. Wambach, *Rev. Mod. Phys.* **81**, 1031 (2009).
  - [2] K. Fukushima and T. Hatsuda, *Rept. Prog. Phys.* **74**, 014001 (2011).
  - [3] K. Fukushima and C. Sasaki, *Prog. Part. Nucl. Phys.* **72**, 99 (2013).
  - [4] S. Borsanyi, *EPJ Web Conf.* **137**, 01006 (2017).
  - [5] P. de Forcrand, *Proc. Sci.*, LAT2009 (2009) 010.
  - [6] C. R. Allton, S. Ejiri, S. J. Hands, O. Kaczmarek, F. Karsch, E. Laermann, C. Schmidt, and L. Scorzato, *Phys. Rev. D* **66**, 074507 (2002).
  - [7] C. R. Allton, S. Ejiri, S. J. Hands, O. Kaczmarek, F. Karsch, E. Laermann, and C. Schmidt, *Phys. Rev. D* **68**, 014507 (2003).
  - [8] S. Ejiri *et al.* (WHOT-QCD Collaboration), *Phys. Rev. D* **82**, 014508 (2010).
  - [9] Z. Fodor and S. D. Katz, *Phys. Lett.* **B534**, 87 (2002).
  - [10] P. de Forcrand and O. Philipsen, *Nucl. Phys.* **B642**, 290 (2002); **B673**, 170 (2003).
  - [11] M. D'Elia and M. P. Lombardo, *Phys. Rev. D* **67**, 014505 (2003); **70**, 074509 (2004).
  - [12] S. Muroya, A. Nakamura, C. Nonaka, and T. Takaishi, *Prog. Theor. Phys.* **110**, 615 (2003).
  - [13] A. Nakamura, S. Oka, and Y. Taniguchi, *JHEP* **1602**, 054 (2016).
  - [14] V. G. Bornyakov, D. L. Voyda, V. A. Goy, A. V. Molochkov, A. Nakamura, A. A. Nikolaev, and V. I. Zakharov, *Phys. Rev. D* **95**, 094506 (2017).
  - [15] G. Aarts, *Phys. Rev. Lett.* **102**, 131601 (2009).
  - [16] G. Aarts, L. Bongiovanni, E. Seiler, D. Sexty, and I. -O. Stamatescu, *Eur. Phys. J. A* **49**, 89 (2013).
  - [17] D. Sexty, *Phys. Lett. B* **729**, 108 (2014).
  - [18] G. Aarts, E. Seiler, D. Sexty, and I. -O. Stamatescu, *Phys. Rev. D* **90**, 114505 (2014).
  - [19] M. Cristoforetti, F. DiRenzo, and L. Scorzato, *Phys. Rev. D* **86**, 074506 (2012).
  - [20] H. Fujii, D. Honda, M. Kato, Y. Kikukawa, S. Komatsu, and T. Sano, *J. High Energy Phys.* **10**, 147 (2013).
  - [21] T. Umeda, K. Nomura, and H. Matsufuru, *Eur. Phys. J C* **37**, s9 (2004).
  - [22] M. Cheng *et al.*, *Eur. Phys. J. C* **71**, 1564 (2011).
  - [23] A. Bazavov *et al.* (HotQCD Collaboration), *Phys. Rev. D* **86**, 094503 (2012).
  - [24] M. Ishii, T. Sasaki, K. Kashiwa, H. Kouno and M. Yahiro, *Phys. Rev. D* **89**, 071901(R) (2014).
  - [25] M. Ishii, K. Yonemura, J. Takahashi, H. Kouno, and M. Yahiro, *Phys. Rev. D* **93**, 016002 (2016).
  - [26] J. Adams *et al.* (STAR Collaboration), *Nucl. Phys.* **A757**, 28 (2005).
  - [27] I. Pushkina *et al.* (QCD-TARO Collaboration), *Phys. Lett.* **B609**, 265 (2005).
  - [28] H. Iida, Y. Maezawa, and K. Yazaki, *Proc. Sci.*, LAT2010 (2010) 189.
  - [29] Y. Maezawa *et al.* (WHOT-QCD Collaboration), *Phys. Rev. D* **75**, 074501 (2007).
  - [30] A. Ali Khan *et al.* (CP-PACS Collaboration), *Phys. Rev. D* **63**, 034502 (2000).
  - [31] A. Ali Khan *et al.* (CP-PACS Collaboration), *Phys. Rev. D* **64**, 074510 (2001).
  - [32] J. Takahashi, H. Kouno, and M. Yahiro, *Phys. Rev. D* **91**, 014501 (2015).
  - [33] A. Roberge and N. Weiss, *Nucl. Phys.* **B275**, 734 (1986).
  - [34] H. Kouno, Y. Sakai, K. Kashiwa, and M. Yahiro, *J. Phys. G* **36**, 115010 (2009).
  - [35] Y. Sakai, K. Kashiwa, H. Kouno, and M. Yahiro, *Phys. Rev. D* **77**, 051901(R) (2008); **78**, 036001 (2008).
  - [36] Y. Sakai, K. Kashiwa, H. Kouno, M. Matsuzaki, and M. Yahiro, *Phys. Rev. D* **78**, 076007 (2008); **79**, 096001 (2009).
  - [37] Y. Sakai, H. Kouno, and M. Yahiro, *J. Phys. G* **37**, 105007 (2010).